Strong mechanical squeezing in a standard optomechanical system by pump modulation

Cheng-Hua Bai,[1] Dong-Yang Wang,[1] Shou Zhang,[1,2,*] Shutian Liu,[1,†] and Hong-Fu Wang[2,‡]
[1]*School of Physics, Harbin Institute of Technology, Harbin, Heilongjiang 150001, China*
[2]*Department of Physics, College of Science, Yanbian University, Yanji, Jilin 133002, China*

(Received 18 November 2019; accepted 28 April 2020; published 15 May 2020)

We propose a simple yet surprisingly effective mechanical squeezing scheme in a standard optomechanical system that is beneficial for the amplitude modulation of the pump laser. By merely introducing a specific kind of periodic modulation into the single-tone driving field to cool down the mechanical Bogoliubov mode, strong mechanical squeezing, far beyond 3 dB, can be engineered without the requirement for any additional techniques. Specifically, we find that the amount of squeezing is not simply dependent on the order of magnitude of the effective optomechanical coupling but strongly on the ratio of sideband strengths for it. To maximize the mechanical squeezing, we numerically and analytically optimize this ratio in the steady-state regime, respectively. The mechanical squeezing engineered in our scheme also is extremely robust and can survive at a high bath temperature. Compared with previous schemes based on the two-tone pump technique, our scheme involves fewer external control laser sources and can be extended to other quantum systems to achieve a strong squeezing effect.

DOI: 10.1103/PhysRevA.101.053836

I. INTRODUCTION

In recent years, with the enormous advances in optomechanics, including the experimental realization of quantum ground-state cooling for mechanical oscillators [1–6] and exploitation of strong optomechanical coupling [7–9], the optomechanical system, the study of a controllable radiation-pressure interaction between optical (microwave) and mechanical degrees of freedom, has been the flexible platform for the quantum manipulation of macroscopic mechanical oscillators in the fields of fundamental research and applied science [10–13]. Particularly, the exploration of the quantum-to-classical transition [11,14], the search for novel quantum effects at the macroscale [15], and the pursuit to measure extremely weak signals (gravitational waves) with an ultrahigh precision at the quantum level of sensitivity [16,17] have been the primary thrust for engineering strong mechanical squeezing in optomechanical systems. Therefore, many significant efforts have been devoted to developing alternative mechanical squeezing methods and techniques. In the early parametric amplification mechanical squeezing scheme, similar to the parametric technique applied to optical squeezing [18], due to the limitation of system instability, the amount of mechanical squeezing could not be reduced to below one-half the standard quantum limit (i.e., the so-called 3-dB limit) [19]. Based on the cavity optomechanical system, many schemes have also been proposed to generate mechanical squeezing, such as modulation of the external driving field [20–22], quantum squeezing transfer from the optical parametric amplifier to the mechanical oscillator [23], and XX-type interaction induced by a mechanical non-Markovian reservoir [24]. Although the above schemes possess respective advantages under certain circumstances, the achieved mechanical squeezing is relatively weak and fails to break the 3-dB limit. As a consequence, to overcome this limit, other strong mechanical squeezing schemes have been proposed accordingly, including squeezed light driving and squeezing transfer [25], quadratic optomechanical coupling [26], dissipative optomechanical coupling [27,28], and Duffing nonlinearity [29–31]. We have also investigated the joint mechanical squeezing effect between two kinds of squeezing techniques instead of only one squeezing manipulation method in the above schemes and found that strong mechanical squeezing, beyond the 3-dB limit, can be easily engineered, but each kind of independent squeezing component is permitted below 3 dB [32]. Furthermore, some schemes have even resorted to more complex techniques, such as quantum measurement [33–35], quantum feedback [36], modulations of radiation-pressure coupling and mechanical spring constant [37], combination of both linear and quadratical optomechanical couplings and squeezed light injection [38], and simultaneous linear and nonlinear couplings and amplitude-modulated driving field [39].

In fact, another powerful approach to effectively manipulate quantum states is reservoir engineering. Due to the advantages of the independence of the initial state for the system and the robustness with respect to decoherence for the environment, this technique is extremely high performance in experimental implementations and has been widely applied in cavity (circuit) quantum electrodynamics [40–44] and cavity optomechanics [45–53]. In Ref. [45], a stationary two-mode squeezed vacuum state of two mechanical oscillators can be generated by cavity dissipation. The highly entangled cavity fields can be achieved by mechanical dissipation in a three-mode optomechanical system where two optical or

*szhang@ybu.edu.cn
†stliu@hit.edu.cn
‡hfwang@ybu.edu.cn

microwave cavity modes are coupled to a common mechanical mode [46]. Very recently, the theoretical work in Ref. [46] has been successfully demonstrated in experiments and the stationary emission of entangled microwave radiation fields was observed [47]. However, Ref. [48] considered a different case where two mechanical oscillators are independently coupled to a common cavity mode and strong mechanical-mechanical entanglement can be prepared by the engineering of a single reservoir. Based on this scheme, the stabilized entanglement between two massive micromechanical oscillators has also been reported experimentally using the technique of reservoir engineering [49]. The typical mechanical squeezing scheme applying the reservoir engineering technique to optomechanics is driving an optical or microwave cavity with a pair of pump tones at $\omega_c \mp \omega_m$ (ω_c is the optical or microwave frequency while ω_m is the mechanical frequency) [50], and it is required that the red-detuned pump should be at a higher power than the blue-detuned pump. Subsequently, utilizing the reservoir engineering technique based on two-tone driving, some experimental works have manipulated a micromechanical oscillator into a quantum squeezed state [51–53]. Hence, a novel and interesting idea arises: Can the above schemes [50–53] work well when there is only a single-tone pump? We wish to address this curious question.

In this paper, we consider a standard optomechanical device involving only one cavity mode and one mechanical mode which are coupled through radiation-pressure interaction. A specific kind of periodic amplitude modulation is introduced into the single-tone driving field. This operation leads to the desired form of effective optomechanical coupling in the long-time limit, which permits cooling down the Bogoliubov mode of the mechanical mode via the interaction with the cavity mode. Under this mechanism, strong mechanical squeezing, far surpassing 3 dB, can be engineered. We discuss in detail the effects of the nonresonant terms induced by the periodic structure of the effective optomechanical coupling on the mechanical squeezing, which results in the direction of quadrature squeezing rotating continuously in phase space. To maximize the squeezing, we numerically and analytically optimize the ratio for the effective optomechanical coupling sideband strengths, respectively, which balances the competing effect between the two opposing tendencies to the greatest degree. We also note that the engineered mechanical squeezing is robust against mechanical thermal noise and can survive at a high bath temperature. Besides involving fewer external control laser sources compared with previous schemes, our scheme can also be generalized to simplify some existing schemes, such as dissipative generation of a squeezed output field [54] and mechanical squeezing in an unresolved-sideband regime [55] based on the two pump tones.

The rest of this paper is organized as follows. In Sec. II, we introduce the standard optomechanical system driven by a periodically amplitude-modulated single-tone pump field. In Sec. III, we illustrate the periodic dynamics of the manipulated optomechanical system and derive the linear quantum Langevin equation. In Sec. IV, we obtain the required effective optomechanical coupling for the generation of mechanical squeezing and discuss it in detail from the perspectives of nonresonant term influence without the rotating-wave approximation (RWA), balancing of the competing effects, and optimization of the ratio for the effective optomechanical coupling sideband strengths, respectively. In Sec. V, via elimination of the cavity mode adiabatically, explicitly analytical expressions for the stationary mechanical squeezing and the optimized ratio for the sideband strengths are obtained and the experimental feasibility is also briefly analyzed. Finally, we summarize our work in Sec. VI.

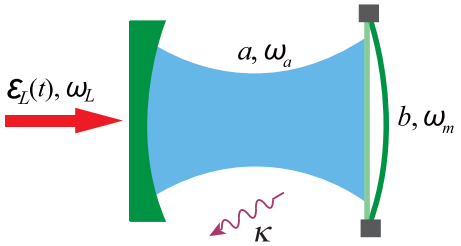

FIG. 1. Schematic of the optomechanical setup for achieving strong mechanical squeezing, where the cavity field driven by a periodically amplitude-modulated external laser field couples to the mechanical mode via the controllable radiation-pressure interaction.

II. MODEL AND HAMILTONIAN

A sketch of the modulated optomechanical system is shown in Fig. 1, in which a periodically amplitude-modulated external driving field [with amplitude $\varepsilon_L(t)$ and frequency ω_L] is imposed on the standard optomechanical system. Under the strong-driving regime, the optical field (with frequency ω_a and decay rate κ) interacts with the mechanical oscillator (with frequency ω_m and damping γ_m) via the manipulable radiation-pressure effect. In the rotating frame with respect to the laser frequency ω_L, the system Hamiltonian can be written as ($\hbar = 1$)

$$H = \delta_a a^\dagger a + \omega_m b^\dagger b - g_0 a^\dagger a(b + b^\dagger) + i[\varepsilon_L(t)e^{i\varphi}a^\dagger - \varepsilon_L^*(t)e^{-i\varphi}a], \quad (1)$$

where $\delta_a = \omega_a - \omega_L$ is the frequency detuning of the cavity with respect to the input laser, $a^\dagger$ ($b^\dagger$) and a (b) are the creation and annihilation operators of the cavity (mechanical) mode, respectively, and g_0 is the single-photon optomechanical coupling strength. $\varepsilon_L(t)$ is the periodically modulated amplitude of the external driving field and is carried out for a modulation period τ, i.e., $\varepsilon_L(t) = \varepsilon_L(t+\tau) = \sum_{n=-\infty}^{\infty} \varepsilon_n e^{-in\Omega t}$, in which $\Omega = 2\pi/\tau$ is the modulation frequency and ε_n is the sideband-modulation strength associated with the corresponding sideband power P_n by $\varepsilon_n = \sqrt{2\kappa P_n/(\hbar\omega_L)}$. φ is the phase of the laser field coupling to cavity mode a [56]. For simplicity, we usually set $\varphi = 0$ in generic optomechanical systems [57,58]. Later we show the extremely vital role that the modulation sidebands ($\sim e^{\pm i\Omega t}$) play in engineering strong mechanical squeezing.

Due to the coupling between the optomechanical system and the environment, the system dynamics will inevitably be influenced by the cavity decay and mechanical damping. Taking these dissipative elements into account, the quantum Langevin equations (QLEs) that dominate the system dynam-

ical evolution are

$$\frac{da}{dt} = -i\delta_a a + ig_0 a(b+b^\dagger) + \varepsilon_L(t) - \frac{\kappa}{2}a + \sqrt{\kappa}a_{\rm in}(t),$$
$$\frac{db}{dt} = -i\omega_m b + ig_0 a^\dagger a - \frac{\gamma_m}{2}b + \sqrt{\gamma_m}b_{\rm in}(t), \quad (2)$$

where $a_{\rm in}(t)$ and $b_{\rm in}(t)$ are, respectively, the zero-mean cavity vacuum input noise operator and mechanical thermal noise operator. Under the Markovian reservoir assumption, the nonzero correlation functions of the noise operators $a_{\rm in}$ and $b_{\rm in}$ are [59]

$$\langle a_{\rm in}^\dagger(t)a_{\rm in}(t')\rangle = n_a\delta(t-t'),$$
$$\langle a_{\rm in}(t)a_{\rm in}^\dagger(t')\rangle = (n_a+1)\delta(t-t'),$$
$$\langle b_{\rm in}^\dagger(t)b_{\rm in}(t')\rangle = n_m\delta(t-t'),$$
$$\langle b_{\rm in}(t)b_{\rm in}^\dagger(t')\rangle = (n_m+1)\delta(t-t'), \quad (3)$$

where n_a and n_m are the mean thermal occupancies of the cavity bath and mechanical bath, respectively.

III. SYSTEM PERIODIC DYNAMICS

Strong external driving induces high amplitudes of the cavity mode and mechanical mode so that the standard linearization technology can be applied to the nonlinear QLEs in Eq. (2). For this purpose, we write cavity mode a and mechanical mode b as the sum of the classical mean value and the quantum fluctuation operator, i.e., $\mathcal{O} \to \langle\mathcal{O}(t)\rangle + \mathcal{O}(\mathcal{O} = a, b)$. In this case, we obtain the set of equations of motion for $\langle a(t)\rangle$ and $\langle b(t)\rangle$:

$$\frac{d\langle a(t)\rangle}{dt} = -i\delta_a\langle a(t)\rangle + ig_0\langle a(t)\rangle[\langle b(t)\rangle + \langle b(t)\rangle^*] + \varepsilon_L(t) - \frac{\kappa}{2}\langle a(t)\rangle,$$
$$\frac{d\langle b(t)\rangle}{dt} = -i\omega_m\langle b(t)\rangle + ig_0|\langle a(t)\rangle|^2 - \frac{\gamma_m}{2}\langle b(t)\rangle. \quad (4)$$

The linearized QLEs for the quantum fluctuation operators can be correspondingly acquired,

$$\frac{da}{dt} = -i\Delta_a a + ig_0\langle a(t)\rangle(b+b^\dagger) - \frac{\kappa}{2}a + \sqrt{\kappa}a_{\rm in}(t),$$
$$\frac{db}{dt} = -i\omega_m b + ig_0\langle a(t)\rangle^* a + ig_0\langle a(t)\rangle a^\dagger - \frac{\gamma_m}{2}b + \sqrt{\gamma_m}b_{\rm in}(t), \quad (5)$$

where $\Delta_a = \delta_a - g_0[\langle b(t)\rangle + \langle b(t)\rangle^*]$ is the effective cavity detuning sightly modulated by the mechanical motion.

Owing to the periodic modulation of the external driving acting on the optomechanical cavity $[\varepsilon_L(t) = \varepsilon_L(t+\tau)]$, according to the Floquet theorem [60], for the present linearized dynamical system, the cavity mode amplitude $\langle a(t)\rangle$ and mechanical mode amplitude $\langle b(t)\rangle$ will acquire the same modulation period with the performed external driving in the asymptotic regime, i.e., $\lim_{t\to\infty}\langle a(t)\rangle = \langle a(t+\tau)\rangle$ and $\lim_{t\to\infty}\langle b(t)\rangle = \langle b(t+\tau)\rangle$.

For simplicity and to produce the desired system dynamics for generating mechanical squeezing, we need only to truncate the driving-modulation sidebands to the order of $e^{\pm i\Omega t}$, i.e., $\varepsilon_L(t) = \sum_{n=-1}^{1}\varepsilon_n e^{-in\Omega t}$. As a result, the cavity mode amplitude $\langle a(t)\rangle$ and mechanical mode amplitude $\langle b(t)\rangle$ will have the same form as the chosen external driving-modulation structure in the long-time limit,

$$\langle\mathcal{O}(t)\rangle = \mathcal{O}_{-1}e^{i\Omega t} + \mathcal{O}_0 + \mathcal{O}_1 e^{-i\Omega t} \ (\mathcal{O} = a, b), \quad (6)$$

where $\mathcal{O}_n$ are the sideband amplitudes for the cavity and mechanical modes with $n = -1, 0, 1$. For more details see Appendix A.

IV. ENGINEERING OF MECHANICAL SQUEEZING

In order to reveal the significantly important effect of the modulation sidebands ($\sim e^{\pm i\Omega t}$) on the engineering mechanical squeezing, we define $g_0\langle a(t)\rangle$ in Eq. (4) as the effective optomechanical coupling $G(t)$ and specify it as

$$G(t) = g_0\langle a(t)\rangle = G_{-1}e^{i\Omega t} + G_0 + G_1 e^{-i\Omega t}, \quad (7)$$

where G_n $(n = -1, 0, 1)$ are time-independent positive reals and associated with the driving sideband components ε_n. By further indicating the slow-varying fluctuation operators with tildes, $a = \tilde{a}e^{-i\Delta_a t}$, $b = \tilde{b}e^{-i\omega_m t}$, $a_{\rm in} = \tilde{a}_{\rm in}e^{-i\Delta_a t}$, and $b_{\rm in} = \tilde{b}_{\rm in}e^{-i\omega_m t}$, setting the effective cavity detuning as the anti-Stokes sideband $\Delta_a = \omega_m$ and the external driving modulation frequency $\Omega = 2\omega_m$, and assuming that the effective optomechanical coupling sideband amplitudes are weak, i.e., $G_n \ll \omega_m$, the linearized QLEs for the operators $\tilde{a}$ and $\tilde{b}$ can be simplified as

$$\dot{\tilde{a}} = iG_0\tilde{b} + iG_1\tilde{b}^\dagger - \frac{\kappa}{2}\tilde{a} + \sqrt{\kappa}\tilde{a}_{\rm in}(t),$$
$$\dot{\tilde{b}} = iG_0\tilde{a} + iG_1\tilde{a}^\dagger - \frac{\gamma_m}{2}\tilde{b} + \sqrt{\gamma_m}\tilde{b}_{\rm in}(t), \quad (8)$$

where the fast-oscillating terms $e^{\pm 2i\omega_m t}$ and $e^{\pm 4i\omega_m t}$ have been omitted safely under the RWA and whose nonresonant effects are discussed later.

For convenience, we indicate the quadrature fluctuation operators with tildes,

$$\delta\widetilde{X}_{\mathcal{O}=a,b} = (\tilde{\mathcal{O}} + \tilde{\mathcal{O}}^\dagger)/\sqrt{2},$$
$$\delta\widetilde{Y}_{\mathcal{O}=a,b} = (\tilde{\mathcal{O}} - \tilde{\mathcal{O}}^\dagger)/\sqrt{2}i, \quad (9)$$

and the quadrature noise operators with tildes,

$$\widetilde{X}^{\rm in}_{\mathcal{O}=a,b} = (\tilde{\mathcal{O}}_{\rm in} + \tilde{\mathcal{O}}^\dagger_{\rm in})/\sqrt{2},$$
$$\widetilde{Y}^{\rm in}_{\mathcal{O}=a,b} = (\tilde{\mathcal{O}}_{\rm in} - \tilde{\mathcal{O}}^\dagger_{\rm in})/\sqrt{2}i. \quad (10)$$

Then Eq. (8) can be expressed in a more concise form,

$$\dot{\widetilde{\mathbf{R}}}(t) = \widetilde{\mathbf{M}}\widetilde{\mathbf{R}}(t) + \widetilde{\mathbf{N}}(t), \quad (11)$$

where the vector $\widetilde{\mathbf{R}}$ for the fluctuation operators is $\widetilde{\mathbf{R}} = [\delta\widetilde{X}_a, \delta\widetilde{Y}_a, \delta\widetilde{X}_b, \delta\widetilde{Y}_b]^T$, the 4×4 time-independent coefficient matrix $\widetilde{\mathbf{M}}$ is

$$\widetilde{\mathbf{M}} = \begin{bmatrix} -\frac{\kappa}{2} & 0 & 0 & -G_- \\ 0 & -\frac{\kappa}{2} & G_+ & 0 \\ 0 & -G_- & -\frac{\gamma_m}{2} & 0 \\ G_+ & 0 & 0 & -\frac{\gamma_m}{2} \end{bmatrix}, \quad (12)$$

and the noise operator victor $\widetilde{\mathbf{N}}$ is defined as $\widetilde{\mathbf{N}} = [\sqrt{\kappa}\widetilde{X}_a^{\rm in}, \sqrt{\kappa}\widetilde{Y}_a^{\rm in}, \sqrt{\gamma_m}\widetilde{X}_b^{\rm in}, \sqrt{\gamma_m}\widetilde{Y}_b^{\rm in}]^T$. Here $G_\pm = G_0 \pm G_1$.

Obviously, Eq. (11), which is completely equivalent to the linearized QLEs in Eq. (8), is a first-order inhomogeneous differential equation with a constant coefficient, whose formal solution can be written as

$$\widetilde{\mathbf{R}}(t) = \widetilde{\mathbf{G}}(t)\widetilde{\mathbf{R}}(0) + \widetilde{\mathbf{G}}(t)\int_0^t \widetilde{\mathbf{G}}^{-1}(\tau)\widetilde{\mathbf{N}}(\tau)d\tau, \tag{13}$$

in which $\widetilde{\mathbf{G}}(t)$ satisfies $\dot{\widetilde{\mathbf{G}}}(t) = \widetilde{\mathbf{M}}\widetilde{\mathbf{G}}(t)$ and its initial condition is $\widetilde{\mathbf{G}}(0) = \mathbf{I}$ (here $\mathbf{I}$ is the identity matrix).

For a more general regime of the optomechanical system, introducing the covariance matrix (CM) is more convenient for study of the dynamical evolution of the system. To this end, we define a CM $\widetilde{\mathbf{V}}(t)$ with components $\widetilde{\mathbf{V}}_{ij}(t) = \langle\widetilde{\mathbf{R}}_i(t)\widetilde{\mathbf{R}}_j(t)\rangle$ for $i, j = 1, 2, 3, 4$. Upon further combining Eq. (13), the explicit expression of the CM $\widetilde{\mathbf{V}}(t)$ is

$$\widetilde{\mathbf{V}}(t) = \widetilde{\mathbf{G}}(t)\widetilde{\mathbf{V}}(0)\widetilde{\mathbf{G}}^T(t) + \widetilde{\mathbf{G}}(t)\widetilde{\mathbf{S}}(t)\widetilde{\mathbf{G}}^T(t), \tag{14}$$

where

$$\widetilde{\mathbf{S}}(t) = \int_0^t\int_0^t \widetilde{\mathbf{G}}^{-1}(\tau)\widetilde{\mathbf{K}}(\tau,\tau')[\widetilde{\mathbf{G}}^{-1}(\tau')]^T d\tau d\tau', \tag{15}$$

in which $\widetilde{\mathbf{K}}(\tau,\tau')$ is the so-called two-time noise correlation function, whose elements are defined as $\widetilde{\mathbf{K}}_{ij}(\tau,\tau') = \langle\widetilde{\mathbf{N}}_i(\tau)\widetilde{\mathbf{N}}_j(\tau')\rangle$. Obviously, the last two diagonal elements, $\widetilde{\mathbf{V}}_{33}(t)$ and $\widetilde{\mathbf{V}}_{44}(t)$, of $\widetilde{\mathbf{V}}(t)$ are just the variances for the mechanical position and momentum, respectively. Certainly, the degree of mechanical squeezing can also be expressed in decibel units by $-10\log_{10}[\widetilde{\mathbf{V}}_{jj}(t)/0.5]$ $(j = 3, 4)$. Here, we specify that the cavity mode a is prepared in the vacuum state while the mechanical mode b is in the thermal state with the occupancy n_m initially.

According to the Routh-Hurwitz stability criterion [61], only if all eigenvalues of the time-independent coefficient matrix $\widetilde{\mathbf{M}}$ in Eq. (11) possess negative real parts will the system dynamics characterized by Eq. (11) finally be stable. For the current parameter regime, the stability constraint can be reduced as a simple form: $G_0 > G_1$.

A. Nonresonant effects without the RWA

In the above discussion, we have ignored the nonresonant effects of the fast-oscillating terms by using the RWA. In this case, their functions in engineering mechanical squeezing are erased. To determine the contributions of the discarded high-frequency oscillating terms, we redefine the quadrature fluctuation operators, the quadrature noise operators, and their corresponding operator vectors without tildes. Their forms are exactly the same as the above definitions except for the time-dependent coefficient matrix $\mathbf{M}(t)$,

$$\mathbf{M}(t) = \begin{bmatrix} -\frac{\kappa}{2} & \Delta_a & -\mathrm{Im}[2G(t)] & 0 \\ -\Delta_a & -\frac{\kappa}{2} & \mathrm{Re}[2G(t)] & 0 \\ 0 & 0 & -\frac{\gamma_m}{2} & \omega_m \\ \mathrm{Re}[2G(t)] & \mathrm{Im}[2G(t)] & -\omega_m & -\frac{\gamma_m}{2} \end{bmatrix}, \tag{16}$$

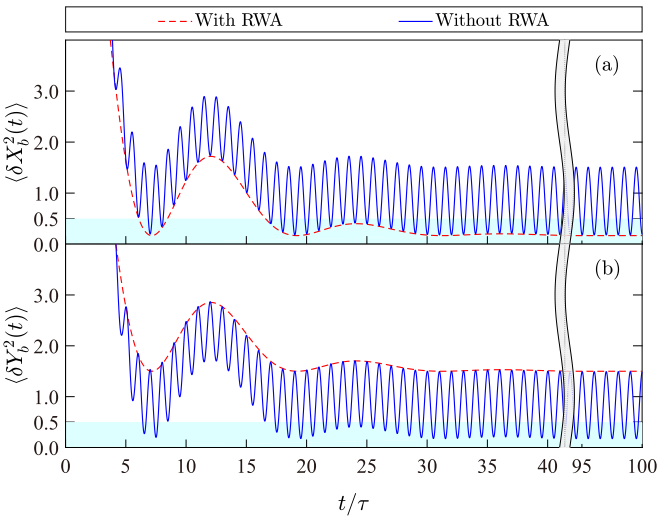

FIG. 2. Time evolution of variances for the mechanical position and momentum fluctuations with and without the RWA, respectively. System parameters are set at $\Delta_a = \omega_m$, $\kappa = 0.1\omega_m$, $\gamma_m = 10^{-6}\omega_m$, $G_{-1} = 0.01\omega_m$, $G_0 = 0.1\omega_m$, $G_1 = 0.05\omega_m$, $n_m = 10$, and $n_a = 0$. The blue-shaded region at the bottom corresponds to mechanical squeezing.

where Re[...] and Im[...] indicate, respectively, the real and imaginary parts of a complex number. As a result, the fluctuation operator vector $\mathbf{R}$ is

$$\mathbf{R}(t) = \mathbf{G}(t)\mathbf{R}(0) + \mathbf{G}(t)\int_0^t \mathbf{G}^{-1}(\tau)\mathbf{N}(\tau)d\tau, \tag{17}$$

where $\mathbf{G}(t)$ fulfills $\dot{\mathbf{G}}(t) = \mathbf{M}(t)\mathbf{G}(t)$ and the initial condition is still $\mathbf{G}(0) = \mathbf{I}$.

To check the dynamics of quadrature squeezing explicitly, in Fig. 2, we display the time evolution of variances for the mechanical position and momentum fluctuations in cases with and without the RWA in the modulation periods of $[0, 100\tau]$ when a typical parameter set of the effective optomechanical coupling sideband strengths (G_{-1}, G_0, G_1) is given. Clearly, it is shown that, when the RWA is not used, the mechanical position and momentum will be periodically squeezed in the long-time limit and the squeezing period is just the performed external modulation period τ. For example, in the modulation periods of $[95\tau, 100\tau]$, the mechanical position and momentum are all squeezed five times, respectively. However, as shown in Fig. 2, due to the bound of the Heisenberg uncertainty relation [62], the mechanical position and momentum cannot be squeezed simultaneously. Once the RWA is exploited to erase the contributions of the high-frequency oscillating terms $e^{\pm 2i\omega_m t}$ and $e^{\pm 4i\omega_m t}$, the τ-periodicity position and momentum squeezing will collapse in the direction of the position and the momentum squeezing will disappear accordingly. But in the cases both with and without the RWA, the amount of mechanical squeezing is almost the same during the entire evolution process.

On the other hand, the nonresonant effects of the fast-oscillating terms can be revealed more intuitively in phase space. To this end, it is necessary to introduce the Wigner function. Due to the above linearized system dynamics [Eq. (5)] and the zero-mean Gaussian nature of the quantum

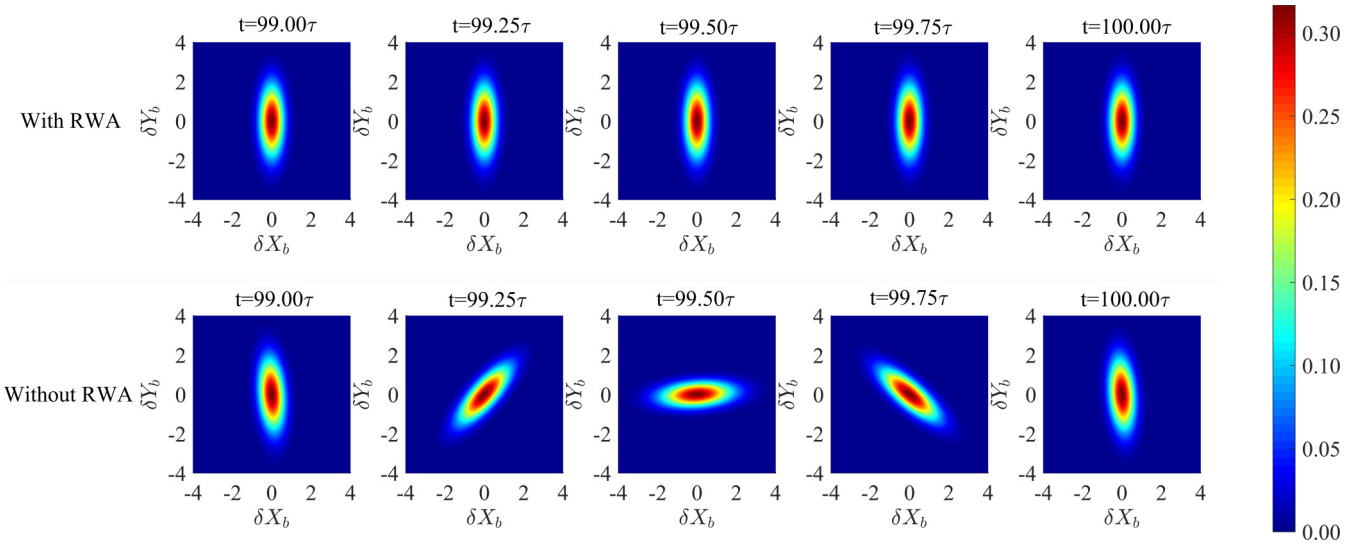

FIG. 3. Wigner functions of the mechanical mode at some different specific times in cases with and without the RWA. System parameters are the same as in Fig. 2.

noises, it ensures that the quantum steady state of the system is a Gaussian state [57,63]. Hence, as long as the CM is obtained, the Wigner function of the mechanical mode can be expressed as [64,65]

$$\mathcal{W}(\mathbf{D}) = \frac{1}{2\pi\sqrt{\mathrm{Det}[\mathbf{V}_b]}}\exp\left\{-\frac{1}{2}\mathbf{D}^T\mathbf{V}_b^{-1}\mathbf{D}\right\}, \tag{18}$$

where $\mathbf{D}$ refers to the two-dimensional vector $\mathbf{D} = [X_b, Y_b]^T$ and $\mathbf{V}_b$ is the CM for the mechanical mode.

In Fig. 3, we further show the Wigner functions of the mechanical mode in the long-time modulation period of $[99\tau, 100\tau]$ for one quarter-period time interval with and without the RWA, respectively. One can observe in Fig. 3 that, under the actions of the nonresonant effects of fast-oscillating terms, the direction of quadrature squeezing rotates continuously in phase space and the rotation period just corresponds to the modulation period τ. This is because the performed external driving is τ periodic $[\varepsilon_L(t) = \varepsilon_L(t+\tau)]$, and according to the Floquet theory, the CM of the system will acquire the same periodicity of the external modulation in the long-time limit, i.e., $\widetilde{\mathbf{V}}(t) = \widetilde{\mathbf{V}}(t+\tau)$ [20,66]. Therefore, from Eq. (18), we can conclude that the Wigner function of the mechanical mode $\mathcal{W}$ will also satisfy $\mathcal{W}(\delta X_b, \delta Y_b, t) = \mathcal{W}(\delta X_b, \delta Y_b, t+\tau)$, and thus the period of rotation of the Wigner function in phase space is 2τ. However, when the high-frequency oscillating terms are omitted by the RWA, the rotation of the Wigner functions at different specific times disappears and they all stretch along the vertical axis and contract along the horizontal axis, which clearly characterizes the mechanical squeezing in the direction of the position. It is also found that, throughout all the Wigner functions in Fig. 3, with or without the RWA, their shape is fixed, which again indicates that the degree of mechanical squeezing is almost equivalent in the two cases. This is since G_0 is maximum in the parameter set (G_{-1}, G_0, G_1), and the Stokes-scattering process $G_0 e^{-2i\omega_m t} ab + G_0 e^{2i\omega_m t} a^\dagger b^\dagger$ is the nearest resonant term among the neglected high-frequency oscillating terms. In the low excitation of the mechanical bath ($n_m = 10$), the quantum backaction effect induced by the nearest resonant Stokes-scattering process on the mechanical mode is very weak. Therefore, the contribution of these high-frequency oscillating terms neglected by the RWA to the shape of the Wigner function is not remarkable.

In addition, to achieve the desired form of the effective optomechanical coupling $G(t)$ as shown in Eq. (7) for a given set (G_{-1}, G_0, G_1), what is of our concern is how to choose an appropriate set of sideband-modulation strengths $(\varepsilon_{-1}, \varepsilon_0, \varepsilon_1)$ for the external driving $\varepsilon_L(t)$. See Appendix B for more details.

In the present mechanical squeezing scheme, if we keep G_0 fixed but add a π phase to G_1, i.e., $G_1 = |G_1|e^{i\pi}$, the quadrature squeezing of the mechanical position and momentum fluctuations in the long-time modulation limit in Fig. 2 will be reversed. As a result, the use of the RWA leads also to squeezing in the direction of momentum and squeezing of the position fluctuation vanishes accordingly.

B. Competing effects between two opposing tendencies

In this subsection, we present further interpretation of engineering mechanical squeezing via dissipation of the cavity mode. For this reason, we introduce the Bogoliubov mode $\beta = \cosh r\tilde{b} + \sinh r\tilde{b}^\dagger$ with $\tanh r = G_1/G_0$. In terms of the Bogoliubov mode, the QLEs in Eq. (8) become

$$\begin{aligned}\dot{\tilde{a}} &= -\frac{\kappa}{2}\tilde{a} + i\mathcal{G}\beta + \sqrt{\kappa}\tilde{a}_{\mathrm{in}}(t),\\ \dot{\beta} &= i\mathcal{G}\tilde{a} - \frac{\gamma_m}{2}\beta + \sqrt{\gamma_m}\beta_{\mathrm{in}}(t),\end{aligned} \tag{19}$$

where $\mathcal{G} = \sqrt{G_0^2 - G_1^2}$ is the effective coupling between the Bogoliubov mode and the cavity mode and $\beta_{\mathrm{in}}(t) = \cosh r\tilde{b}_{\mathrm{in}}(t) + \sinh r\tilde{b}_{\mathrm{in}}^\dagger(t)$ is the effective noise corresponding to the Bogoliubov mode.

In Fig. 4, we plot the position variance $\langle \delta\widetilde{X}_b^2 \rangle$ of the mechanical mode and the occupancy $\langle \beta^\dagger\beta \rangle$ of the Bogoliubov

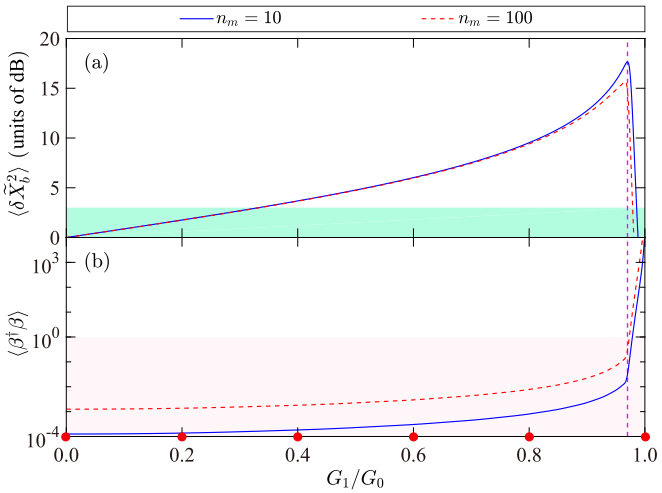

FIG. 4. (a) Position variance $\langle \delta \widetilde{X}_b^2 \rangle$ of the mechanical mode b and (b) occupancy $\langle \beta^\dagger \beta \rangle$ of the Bogoliubov mode β versus the ratio G_1/G_0 of the sideband strengths for the effective optomechanical coupling G in the long-time limit. In both panels, the solid blue and dashed red curves correspond to the results obtained with $n_m = 10$ and $n_m = 100$, respectively. The green- and pink-shaded regions at the bottom in (a) and (b) correspond, respectively, to mechanical squeezing below the 3-dB limit and Bogoliubov mode cooling for $\langle \beta^\dagger \beta \rangle < 1$. The vertical dashed magenta line corresponds to the position of the maximal $\langle \delta \widetilde{X}_b^2 \rangle$ (dB) in the range $G_1 \in [0, G_0]$. System parameters are the same as in Fig. 2.

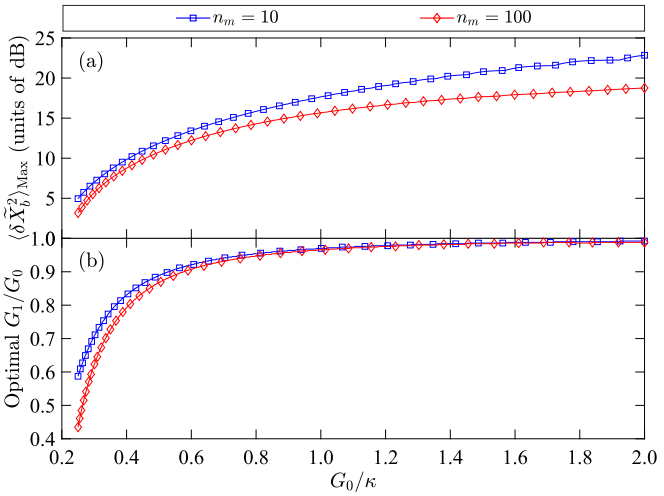

FIG. 5. (a) Maximized position variance $\langle \delta \widetilde{X}_b^2 \rangle$ of the mechanical mode and (b) optimal ratio G_1/G_0 as functions of the effective optomechanical coupling center sideband strength G_0 for different mean thermal occupancies of the mechanical bath. Here the maximized $\langle \delta \widetilde{X}_b^2 \rangle$ in (a) is acquired utilizing the corresponding optimal radio G_1/G_0 in (b) for different G_0 values. System parameters are the same as in Fig. 2.

mode as functions of the effective optomechanical coupling sideband strength ratio G_1/G_0 for a fixed G_0 in the case of different mean bath phonon numbers. It can be found that, in the two cases $n_m = 10$ and $n_m = 100$, with an increase in G_1 up to a critical value, $\langle \delta \widetilde{X}_b^2 \rangle$ is a monotonic function of G_1/G_0 and the mechanical squeezing becomes stronger and stronger. In this corresponding range of G_1/G_0, the occupancy $\langle \beta^\dagger \beta \rangle$ for the Bogoliubov mode increases, but very gently, and the Bogoliubov mode remains in the ground-state cooling zone. However, with a continuous increase in G_1, once beyond this critical value, $\langle \delta \widetilde{X}_b^2 \rangle$ declines rapidly, but on the contrary, $\langle \beta^\dagger \beta \rangle$ increases sharply. One can also clearly see that, for this specific G_1/G_0, $\langle \delta \widetilde{X}_b^2 \rangle$ takes the maximum and $\langle \beta^\dagger \beta \rangle$ simultaneously begins to increase sharply. This interesting competing effect can be thoroughly understood as follows.

According to Eq. (19), in terms of the Bogoliubov mode β, the system Hamiltonian becomes

$$\mathcal{H} = -\mathcal{G}(\tilde{a}\beta^\dagger + \text{H.c.}). \tag{20}$$

This shows that, obviously, the cavity mode $\tilde{a}$ and the Bogoliubov mode β are coupled via the well-known beam-splitter Hamiltonian, which is usually applied to the optomechanical sideband cooling schemes of the mechanical mode [67–69]. Therefore, the Bogoliubov mode β can be cooled into the ground state via the interaction with the cavity mode $\tilde{a}$. With an increase in G_1 for a fixed G_0, the squeezing parameter $r = \text{arctanh}[G_1/G_0]$ will be increased accordingly. Hence, as shown in Fig. 4(a), the mechanical mode is squeezed more strongly. On the other hand, with a continuous increase in G_1, the effective coupling between the cavity mode and the Bogoliubov mode $\mathcal{G} = \sqrt{G_0^2 - G_1^2}$ will be decreased for a fixed G_0 and finally vanish, which inhibits the ground-state cooling of the Bogoliubov mode more and more remarkably. So, as shown in Fig. 4(b), the occupancy $\langle \beta^\dagger \beta \rangle$ rises gently at first and then increases sharply later. Once the Bogoliubov mode β cannot be cooled close to its ground state, the deleterious effect of the thermal noise plays a dominant role and the amount of mechanical squeezing decreases quickly and ultimately disappears. Thus, the strongest mechanical squeezing for a fixed G_0 is just the balanced result from the competing effect of these two different kinds of opposing tendencies. The above novel phenomena verify again the fact that the cooling is a prerequisite to reveal the macroscopic quantum effects of the mechanical mode.

C. Optimal ratio for the effective optomechanical coupling sideband strengths

As illustrated in Fig. 4, for a fixed G_0, there is a specific G_1 that ensures maximization of the mechanical squeezing. If G_1 is small, the mechanical squeezing is weak (r is small). However, when G_1 is too large, the cooling capacity of the cavity mode is restrained significantly. Therefore, to engineer strong mechanical squeezing, it is absolutely necessary to optimize the ratio G_1/G_0 over an appropriate range of G_0.

To this end, we numerically optimize the mechanical position variance $\langle \delta \widetilde{X}_b^2 \rangle$ and the maximized $\langle \delta \widetilde{X}_b^2 \rangle$ as functions of G_0 with different mechanical bath mean occupancies as shown in Fig. 5(a). Meanwhile, the corresponding optimal ratio G_1/G_0 which balances the competing effect between squeezing and cooling best for every G_0 is also presented in Fig. 5(b). As expected, in Fig. 5(a) one can note that, due to the adverse effect of the mechanical thermal noise, this is a reverse dependence of the maximized $\langle \delta \widetilde{X}_b^2 \rangle$ on the mean thermal occupancy of the mechanical bath. On the other hand, with an increase in G_0, the coupling $\mathcal{G} = \sqrt{G_0^2 - G_1^2} =$

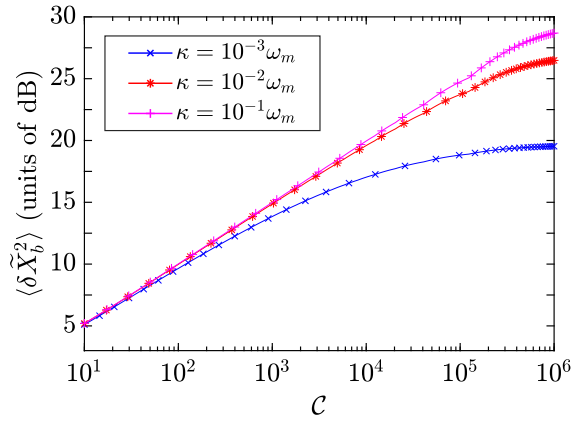

FIG. 6. Position variance $\langle \delta \widetilde{X}_b^2 \rangle$ of the mechanical mode versus the system cooperativity $\mathcal{C}$ with different cavity mode dissipation rates κ, in which $\langle \delta \widetilde{X}_b^2 \rangle$ is obtained with the numerically optimized ratio G_1/G_0. Here the system parameters are chosen as $\gamma_m = 10^{-5}\omega_m$ and $n_m = 0$. Other parameters are the same as in Fig. 2.

$G_0\sqrt{1-(G_1/G_0)^2}$ will be enhanced accordingly for a specific G_1/G_0. As a result, the cooling behavior performed by the cavity mode is more powerful, which means that, as demonstrated in Fig. 5(b), the tendency of the optimal ratio G_1/G_0 is to approach closer and closer to unity but not equal unity. This implies in turn the stronger mechanical squeezing displayed in Fig. 5(a).

In addition, it is well known that the ground-state cooling of the Bogoliubov mode β not only is dependent on the coupling strength $\mathcal{G}$ between the cavity mode and the Bogoliubov mode, but also is related closely to the decay rate of the cavity mode itself. To shed light on the effect of the cavity mode decay rate on engineering mechanical squeezing clearly, in Fig. 6 we plot the position variance $\langle \delta \widetilde{X}_b^2 \rangle$ as functions of the system cooperativity $\mathcal{C} = 4G_0^2/(\kappa\gamma_m)$ with a different decay rate κ, where $\langle \delta \widetilde{X}_b^2 \rangle$ has been maximized by numerically optimizing the ratio over the entire G_1/G_0. One finds that stronger mechanical squeezing can be engineered in the limit of large system cooperativity $\mathcal{C}$. On the other hand, it is also clearly shown that the increasing decay rate of the cavity mode leads to stronger mechanical squeezing.

V. ANALYTICAL SOLUTION FOR THE STEADY-STATE MECHANICAL SQUEEZING

In the present scheme, although we make use of the time-modulated input field to drive the optomechanical system [essentially, it is time modulated for the effective optomechanical coupling $G(t)$], as shown in Sec. IV, the time-dependent system dynamics [Eq. (5)] can be successfully transformed into time-independent effective system dynamics [Eq. (19)] via use of the RWA. Then based on the time-independent effective system dynamics after use of the RWA, as long as the condition of adiabatic approximation is satisfied, i.e., the cavity decay rate κ is much larger than the effective coupling $\mathcal{G}$ between the cavity mode $\tilde{a}$ and the Bogoliubov mode β ($\kappa \gg \mathcal{G}$), the cavity mode $\tilde{a}$ still can be adiabatically eliminated from the dynamics [23].

In this section, to better understand the mechanical squeezing effect and obtain the explicit optimal ratio of G_1/G_0, we analytically solve the position variance of the mechanical mode in the steady regime. From Eq. (19) we obtain

$$\tilde{a} \simeq \frac{2i\mathcal{G}}{\kappa}\beta + \frac{2}{\sqrt{\kappa}}\tilde{a}_{\rm in}(t), \tag{21}$$

and substituting this into Eq. (19), we have

$$\dot{\beta} \simeq -h\beta + \frac{2i\mathcal{G}}{\sqrt{\kappa}}\tilde{a}_{\rm in}(t) + \sqrt{\gamma_m}\beta_{\rm in}(t), \tag{22}$$

where $h = 2\mathcal{G}^2/\kappa + \gamma_m/2$. From Eq. (22), the dynamical equation for the position fluctuation operator δQ_β of the Bogoliubov mode can be obtained,

$$\delta\dot{Q}_\beta = -h\delta Q_\beta + \mathcal{F}_1(t) + \mathcal{F}_2(t), \tag{23}$$

where

$$\mathcal{F}_1(t) = -\frac{2\mathcal{G}}{\sqrt{\kappa}}\widetilde{Y}_a^{\rm in}(t),$$
$$\mathcal{F}_2(t) = \sqrt{\frac{\gamma_m}{2}}[\beta_{\rm in}(t) + \beta_{\rm in}^\dagger(t)] \tag{24}$$

are the effective quantum Langevin forces acting on the Bogoliubov mode and their correlation functions are

$$\langle \mathcal{F}_1(t)\mathcal{F}_1(t')\rangle = \frac{4\mathcal{G}^2}{\kappa}\left(n_a + \frac{1}{2}\right)\delta(t-t'),$$
$$\langle \mathcal{F}_2(t)\mathcal{F}_2(t')\rangle = \gamma_m e^{2r}\left(n_m + \frac{1}{2}\right)\delta(t-t'). \tag{25}$$

According to Eqs. (23) and (25), the dynamical equation for $\langle \delta Q_\beta^2 \rangle$ is

$$\frac{d}{dt}\langle \delta Q_\beta^2\rangle = -2h\langle \delta Q_\beta^2\rangle + \frac{4\mathcal{G}^2}{\kappa}\left(n_a + \frac{1}{2}\right) + \gamma_m e^{2r}\left(n_m + \frac{1}{2}\right), \tag{26}$$

and therefore the analytical solution of $\langle \delta Q_\beta^2 \rangle$ in the steady-state regime is

$$\langle \delta Q_\beta^2\rangle_{\rm s} = \frac{2\mathcal{G}^2}{h\kappa}\left(n_a + \frac{1}{2}\right) + \frac{\gamma_m}{2h}e^{2r}\left(n_m + \frac{1}{2}\right). \tag{27}$$

As a result, the analytical solution for the steady-state position variance $\langle \delta \widetilde{X}_b^2 \rangle_{\rm s}$ of the mechanical mode can be obtained accordingly:

$$\langle \delta \widetilde{X}_b^2\rangle_{\rm s} = e^{-2r}\langle \delta Q_\beta^2\rangle_{\rm s}$$
$$= \frac{2\mathcal{G}^2}{h\kappa}e^{-2r}\left(n_a + \frac{1}{2}\right) + \frac{\gamma_m}{2h}\left(n_m + \frac{1}{2}\right). \tag{28}$$

Here, we consider two limit cases. When $G_1 \to 0$, we obtain $\mathcal{G} \to G_0$, $r = \text{arctanh}G_1/G_0 \to 0$, and $h \to 2G_0^2/\kappa + \gamma_m/2 \simeq 2G_0^2/\kappa$. Therefore,

$$\lim_{G_1\to 0}\langle \delta \widetilde{X}_b^2\rangle_{\rm s} = \left(n_a + \frac{1}{2}\right) + \frac{\kappa\gamma_m}{4G_0^2}\left(n_m + \frac{1}{2}\right). \tag{29}$$

Under the conditions of a high-frequency optical bath ($n_a = 0$) and a large system cooperativity $\mathcal{C}$, $\lim_{G_1\to 0}\langle \delta \widetilde{X}_b^2\rangle \simeq \frac{1}{2}$ (0 dB), which indicates that the mechanical mode is in the vacuum state approximately and it closely coincides with the case of

$G_1 \to 0$ in Fig. 4(a). Obviously, for $G_1 \to G_0$, we obtain $\mathcal{G} \to 0$, $r = \text{arctanh}G_1/G_0 \to \infty$, and $h \to \gamma_m/2$. Hence,

$$\lim_{G_1 \to G_0} \langle \delta \widetilde{X}_b^2 \rangle_{\rm s} = n_m + \frac{1}{2}, \tag{30}$$

which means that the cooling effect disappears completely and the mechanical mode is in a thermal state. This also matches very well the situation of $G_1 \to G_0$ in Fig. 4.

To check the accuracy of the analytical solution in Eq. (28) obtained under the adiabatic approximation, we now solve the exact numerical solution for the steady-state position variance $\langle \delta \widetilde{X}_b^2 \rangle_{\rm s}$ of the mechanical mode. Taking the Fourier transform on both sides of Eq. (11) by $f(t) = \frac{1}{2\pi}\int_{-\infty}^{\infty} f(\omega) e^{-i\omega t} d\omega$ and solving it in the frequency domain, we get the expression for the position fluctuation of the mechanical mode,

$$\begin{aligned} \delta \widetilde{X}_b(\omega) = {} & A(\omega)\widetilde{X}_a^{\rm in}(\omega) + B(\omega)\widetilde{Y}_a^{\rm in}(\omega) \\ & + E(\omega)\widetilde{X}_b^{\rm in}(\omega) + F(\omega)\widetilde{Y}_b^{\rm in}(\omega), \end{aligned} \tag{31}$$

where

$$\begin{aligned} & A(\omega) = 0, \quad B(\omega) = -\frac{4G_-\sqrt{\kappa}}{4G_-G_+ + (\gamma_m - 2i\omega)(\kappa - 2i\omega)}, \\ & E(\omega) = \frac{2(\kappa - 2i\omega)\sqrt{\gamma_m}}{4G_-G_+ + (\gamma_m - 2i\omega)(\kappa - 2i\omega)}, \quad F(\omega) = 0. \end{aligned} \tag{32}$$

Apparently, the contribution of the first two terms in Eq. (31) originates from the optical bath vacuum input noise, while the last two terms correspond to the contribution of the mechanical bath thermal noise. When the effective optomechanical coupling sideband strengths satisfy $G_1 = G_0$, $\delta \widetilde{X}_b(\omega) = \frac{\sqrt{\gamma_m}}{\frac{\gamma_m}{2} - i\omega}\widetilde{X}_b^{\rm in}(\omega)$. Not surprisingly, this shows that the mechanical oscillator will make quantum Brownian motion because of the coupling with the bath environment.

The correlation functions of the noise operators in Eq. (31) are

$$\begin{aligned} \langle \widetilde{X}_a^{\rm in}(\omega)\widetilde{X}_a^{\rm in}(\Omega)\rangle &= \langle \widetilde{Y}_a^{\rm in}(\omega)\widetilde{Y}_a^{\rm in}(\Omega)\rangle \\ &= \left(n_a + \tfrac{1}{2}\right)2\pi\delta(\omega + \Omega), \\ \langle \widetilde{X}_a^{\rm in}(\omega)\widetilde{Y}_a^{\rm in}(\Omega)\rangle &= -\langle \widetilde{Y}_a^{\rm in}(\omega)\widetilde{X}_a^{\rm in}(\Omega)\rangle = i\pi\delta(\omega + \Omega), \\ \langle \widetilde{X}_b^{\rm in}(\omega)\widetilde{X}_b^{\rm in}(\Omega)\rangle &= \langle \widetilde{Y}_b^{\rm in}(\omega)\widetilde{Y}_b^{\rm in}(\Omega)\rangle \\ &= \left(n_m + \tfrac{1}{2}\right)2\pi\delta(\omega + \Omega), \\ \langle \widetilde{X}_b^{\rm in}(\omega)\widetilde{Y}_b^{\rm in}(\Omega)\rangle &= -\langle \widetilde{Y}_b^{\rm in}(\omega)\widetilde{X}_b^{\rm in}(\Omega)\rangle = i\pi\delta(\omega + \Omega), \end{aligned} \tag{33}$$

and the position fluctuation spectrum of the mechanical mode is defined as

$$2\pi S_{\widetilde{X}_b}(\omega)\delta(\omega + \Omega) = \tfrac{1}{2}[\langle \delta\widetilde{X}_b(\omega)\delta\widetilde{X}_b(\Omega)\rangle + \langle \delta\widetilde{X}_b(\Omega)\delta\widetilde{X}_b(\omega)\rangle]. \tag{34}$$

Resorting to Eq. (33), the position fluctuation spectrum $S_{\widetilde{X}_b}$ can be obtained:

$$\begin{aligned} S_{\widetilde{X}_b}(\omega) = {} & [A(\omega)A(-\omega) + B(\omega)B(-\omega)]\left(n_a + \tfrac{1}{2}\right) \\ & + [E(\omega)E(-\omega) + F(\omega)F(-\omega)]\left(n_m + \tfrac{1}{2}\right). \end{aligned} \tag{35}$$

In the case of $G_1 = G_0$, the position fluctuation spectrum is simplified as $S_{\widetilde{X}_b}(\omega) = \gamma_m(n_m + \frac{1}{2})/(\frac{\gamma_m^2}{4} + \omega^2)$, which obviously represents a Lorentzian spectrum with a single peak located at frequency 0 and full width γ_m at half-maximum. The steady-state position variance $\langle \delta \widetilde{X}_b^2 \rangle_{\rm s}$ can be calculated by

$$\langle \delta \widetilde{X}_b^2 \rangle_{\rm s} = \frac{1}{2\pi}\int_{-\infty}^{\infty} S_{\widetilde{X}_b}(\omega) d\omega. \tag{36}$$

Under the condition $G_1 = G_0$, we find $\langle \delta \widetilde{X}_b^2 \rangle_{\rm s} = n_m + \frac{1}{2}$, which is just the case of the analytical solution in Eq. (30).

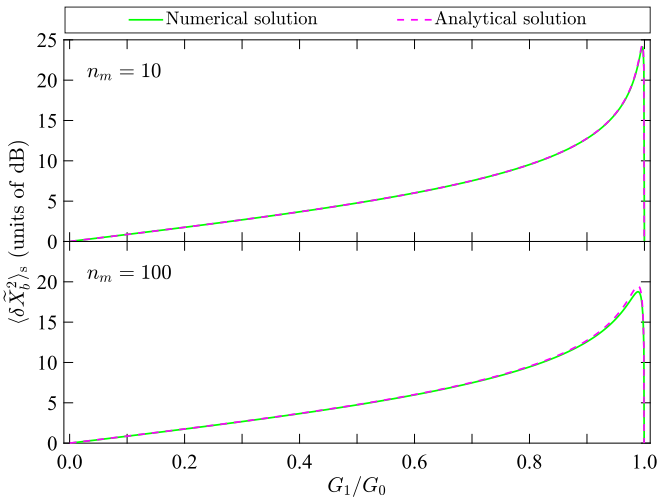

FIG. 7. Comparison between the exact numerical solution and the approximate analytical solution for the steady-state position variance $\langle \delta \widetilde{X}_b^2 \rangle_{\rm s}$ of the mechanical mode with different mechanical bath mean phonon numbers. The solid green and dashed pink curves refer to the results obtained with, respectively, Eqs. (36) and (28). Here the system parameter is chosen as $G_0 = 0.2\omega_m$ and other parameters are the same as in Fig. 2.

In Fig. 7, we compare the steady-state position variance $\langle \delta \widetilde{X}_b^2 \rangle_{\rm s}$ of the mechanical mode obtained from, respectively, the exact numerical solution of Eq. (36) and the approximate analytical solution of Eq. (28) with different mechanical bath mean phonon numbers. As confirmed in Fig. 7, the analytical solution under the adiabatic approximation agrees very well with the exact numerical result.

Once the analytical solution of the steady-state position variance $\langle \delta \widetilde{X}_b^2 \rangle_{\rm s}$ is obtained, the analytical optimal ratio G_1/G_0 to maximize $\langle \delta \widetilde{X}_b^2 \rangle_{\rm s}$ can be evaluated accordingly, in principle, by

$$\frac{d\langle \delta \widetilde{X}_b^2 \rangle_{\rm s}}{d(G_1/G_0)} = 0. \tag{37}$$

After some simplifications, the optimal G_1/G_0 fulfills

$$(1 + 2n_m)\frac{G_1}{G_0}\bigg|_{\rm opt} - \mathcal{C}\left[1 - \left(\frac{G_1}{G_0}\bigg|_{\rm opt}\right)^2\right] e^{-2\text{arctanh}\frac{G_1}{G_0}\big|_{\rm opt}} = 0, \tag{38}$$

which is a transcendental equation for $(G_1/G_0)|_{\rm opt}$ whose analytical solution is hard to solve. However, if we further make an approximation with a large enough cooperativity ($\mathcal{C} \gg 1$)

$$e^{-2r} \simeq \frac{1}{2}\sqrt{\frac{1 + 2n_m}{\mathcal{C}}}, \tag{39}$$

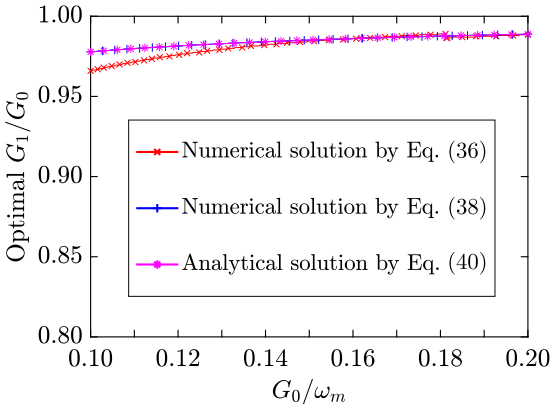

FIG. 8. Optimal ratio G_1/G_0 versus effective optomechanical coupling center sideband strength G_0, where $(G_1/G_0)|_{\rm opt}$ is evaluated with, respectively, the numerical solution of Eq. (36), numerical solution of Eq. (38), and analytical solution of Eq. (40). Here $n_m = 100$ and other parameters are the same as in Fig. 2.

the optimal G_1/G_0 can be obtained analytically:

$$\left.\frac{G_1}{G_0}\right|_{\rm opt} \simeq \sqrt{1+\frac{1+2n_m}{\mathcal{C}}}-\sqrt{\frac{1+2n_m}{\mathcal{C}}}. \tag{40}$$

In Fig. 8, we plot the optimal G_1/G_0 as functions of G_0 using different methods, i.e., numerical solution of Eq. (36), numerical solution of Eq. (38), and analytical solution of Eq. (40). One can note that there is only a little discrepancy among these results initially and they all finally converge. Therefore, the analytical solution of Eq. (40) is approximately valid.

To further show the robustness of the mechanical squeezing engineered via the present method against mechanical thermal noise, we plot the steady-state position variance $\langle\delta\widetilde{X}_b^2\rangle_{\rm s}$ obtained by, respectively, the numerical solution of Eq. (36) and analytical solution of Eq. (28), as a function of the thermal phonon occupation number n_m. As demonstrated in Fig. 9, when the bath temperature is low ($n_m \sim 10$), strong

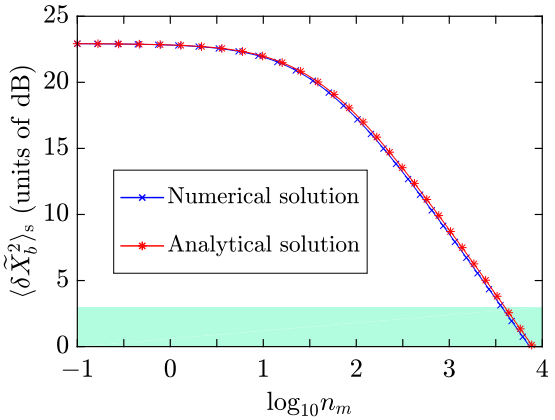

FIG. 9. Position variance $\langle\delta\widetilde{X}_b^2\rangle_{\rm s}$ versus thermal phonon occupation number n_m. The green-shaded region at the bottom corresponds to mechanical squeezing below the 3-dB limit. Here $\gamma_m = 0.5\times10^{-6}\omega_m$, $G_0 = 0.1\omega_m$, and $G_1 = 0.99G_0$. Other system parameters are the same as in Fig. 2.

mechanical squeezing (∼22 dB), far beyond the 3-dB limit, is achievable. The result also shows that the engineered squeezing is extremely robust. Even at a high bath temperature with $n_m \sim 3\times10^3$, the steady-state mechanical squeezing can still break the 3-dB limit. Additionally, one can clearly note that the analytical result is in excellent agreement with the numerical calculation.

Before concluding, we briefly discuss the experimental feasibility of our mechanical squeezing scheme. In the present scheme, the optomechanical setup used is a standard optomechanical cavity, which is significantly common in current cavity optomechanics [10]. The required system parameters are also in an accessible range for existing optomechanical experiments. The applied technique of periodically modulating the driving field has been highly mature until now and is widely used to manipulate optomechanical (electromechanical) systems [20,66,70,71]. Therefore, our squeezing scheme is remarkably workable with the current optomechanics techniques.

VI. CONCLUSIONS

In conclusion, we have proposed a simple but very effective method to engineer strong mechanical squeezing, far surpassing 3 dB, in a standard optomechanical system which only contains a cavity mode and a mechanical mode. The introduction of suitable periodic modulation into the amplitude of the single-tone driving field enables us to obtain the desired form of effective optomechanical coupling, which contributes to cooling the Bogoliubov mode of the mechanical mode close to its ground state resorting to the interaction with the cavity mode. We analyze the role that the nonresonant terms produced by the periodically modulated effective optomechanical coupling in engineering squeezing play and find that they lead to continuous τ-periodicity rotation of the direction of quadrature squeezing in phase space. We demonstrate that the degree of squeezing relies not simply on the magnitude of the effective optomechanical coupling but greatly on the sideband strength ratio G_1/G_0. It is shown that the engineered squeezing is a nonmonotonic function of G_1/G_0. Maximized squeezing results when the optimized G_1/G_0 arranges the competing effect between the squeezing of the mechanical mode and the cooling of the Bogoliubov mode to the best trade-off. In the steady-state regime, we both maximize the squeezing and optimize the ratio G_1/G_0 numerically and analytically, and the results agree very well with each other. We also show that the engineered squeezing is extremely robust against thermal noise and the periodic effective optomechanical coupling form required in our scheme can be precisely prepared via the explicit external single-tone driving field, which indicates that the present scheme is completely feasible with the available experimental platforms in current cavity optomechanics. Compared with previous schemes, our scheme not only involves fewer control laser sources, but also can be expected to simplify some existing schemes based on the two-tone pump driving technique.

ACKNOWLEDGMENTS

This work was supported by the National Natural Science Foundation of China under Grants No. 61822114, No.

61575055, No. 11465020, and No. 61465013 and The Project of Jilin Science and Technology Development for Leading Talent of Science and Technology Innovation in Middle and Young and Team Project under Grant No. 20160519022JH.

APPENDIX A: ASYMPTOTIC EVOLUTION OF THE AMPLITUDES OF THE CAVITY AND MECHANICAL MODES

In the text, we illustrated that when the performed external periodic driving is set at $\varepsilon_L(t) = \varepsilon_{-1}e^{i\Omega t} + \varepsilon_0 + \varepsilon_1 e^{-i\Omega t}$, the amplitudes of the cavity and mechanical modes will evolve toward the same structure in the long-time limit. To gain more insights into this kind of asymptotic process in dynamics, we verify it here using the analytical expressions.

In the parameter regime $g_0 \ll \omega_m$, the optomechanical coupling coefficient g_0 in Eq. (4) can be treated as a perturbation. Meanwhile, due to the periodicity of the implemented driving [$\varepsilon_L(t) = \varepsilon_L(t+\tau)$], the asymptotic amplitudes $\langle a(t)\rangle$ and $\langle b(t)\rangle$ will also be τ periodic. Therefore, the asymptotic solutions of Eq. (4) can be made by double expansions (perturbation expansion and Fourier expansion),

$$\langle \mathscr{O}(t)\rangle = \sum_{j=0}^{\infty}\sum_{n=-\infty}^{\infty} \mathscr{O}_{n,j} e^{in\Omega t} g_0^j \quad (\mathscr{O} = a, b), \tag{A1}$$

where the expansion coefficient $\mathscr{O}_{n,j}$ is time independent. Substituting the above equation into Eq. (4), the zeroth-order perturbation coefficients can be obtained,

$$a_{n,0} = \frac{E_{-n}}{i(\delta_a + n\Omega) + \frac{\kappa}{2}}, \quad b_{n,0} = 0, \tag{A2}$$

and the jth-order perturbation coefficients ($j \geqslant 1$) can also be determined in the following way using recursive relations:

$$a_{n,j} = i\sum_{k=0}^{j-1}\sum_{m=-\infty}^{\infty} \frac{a_{n+m,j-k-1}b^*_{m,k} + a_{n-m,j-k-1}b_{m,k}}{i(\delta_a + n\Omega) + \frac{\kappa}{2}},$$

$$b_{n,j} = i\sum_{k=0}^{j-1}\sum_{m=-\infty}^{\infty} \frac{a_{n+m,j-k-1}a^*_{m,k}}{i(\omega_m + n\Omega) + \frac{\gamma_m}{2}}. \tag{A3}$$

Therefore, the sideband amplitudes $\mathscr{O}_n$ in Eq. (6) can be expressed as

$$\mathscr{O}_n = \sum_{j=0}^{\infty} \mathscr{O}_{-n,j} g_0^j \quad (n = -1, 0, 1). \tag{A4}$$

To verify the validity of the structure as shown in Eq. (6) in the long-time limit, in Fig. 10 we explicitly present the time evolution of the system amplitudes $\langle a(t)\rangle$ and $\langle b(t)\rangle$ in the modulation periods of $[0, 200\tau]$ with the exact numerical solution of Eq. (4) and the analytical expression of Eq. (6), respectively. The left-hand side of each panel in Fig. 10 clearly exhibits the slowly approaching process in dynamics between these two different kinds of results. However, from the right-hand sides, it is surprisingly found that these two kinds of results converge perfectly in long-time modulation periods ($[190\tau, 200\tau]$). Therefore, the cavity mode amplitude $\langle a(t)\rangle$ and the mechanical mode amplitude $\langle b(t)\rangle$ do indeed have the same structure with externally performed driving modulation and are τ periodic in the long-time limit. Moreover, in Fig. 10 one can also clearly see that the τ-periodic asymptotic process

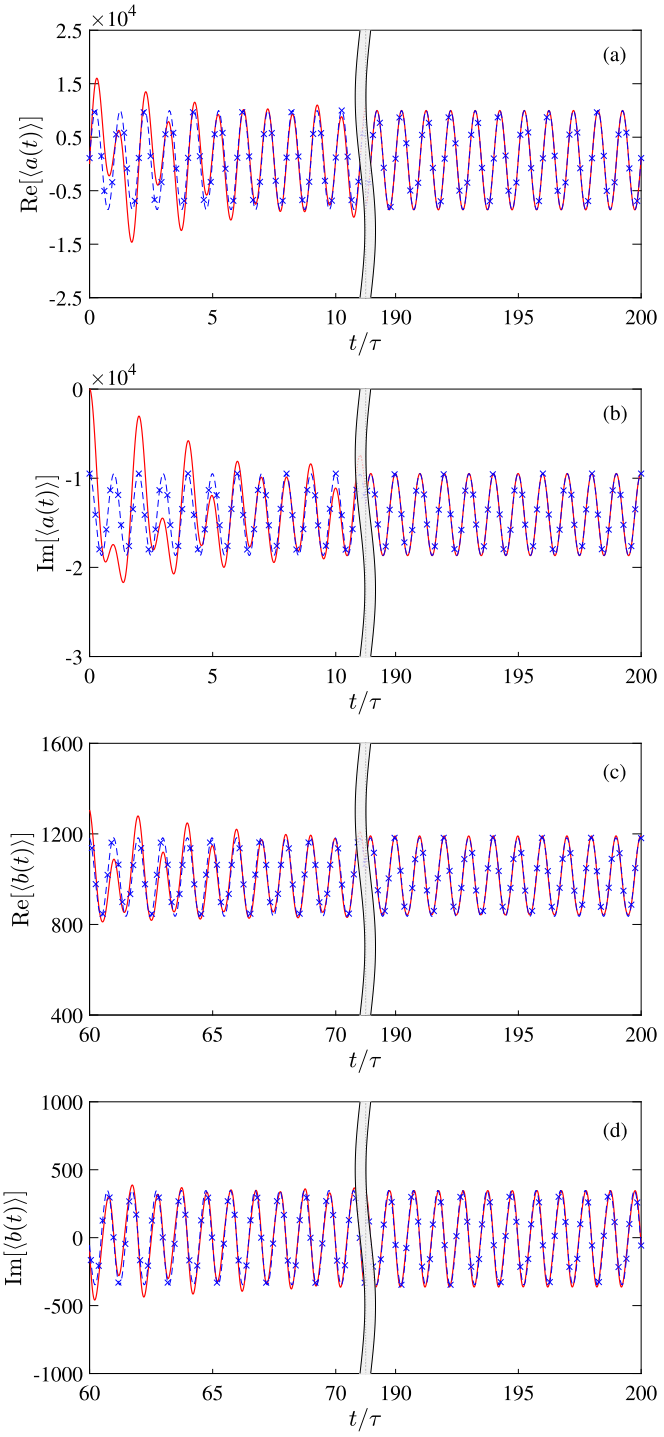

FIG. 10. Asymptotic time evolution of the system amplitudes in the modulation periods of $[0, 200\tau]$. Real and imaginary parts of the cavity mode amplitude $\langle a(t)\rangle$ [mechanical mode amplitude $\langle b(t)\rangle$] versus modulation time t, respectively, in (a) and (b) [(c) and (d)]. In all panels, the solid red and dashed blue cross lines are the results obtained from, respectively, the numerical solution in Eq. (4) and the analytical expression in Eq. (6). System parameters are chosen as (in units of ω_m) $\gamma_m = 10^{-6}$, $\delta_a = 1$, $\kappa = 0.1$, $g_0 = 4\times10^{-6}$, $\varepsilon_0 = 1.4\times10^4$, and $\varepsilon_{\pm1} = 0.7\times10^4$.

of the cavity mode amplitude is much faster than that of the mechanical mode amplitude. This is because the external periodic driving is directly performed on the cavity mode, while the asymptotic τ periodicity of the mechanical mode is obtained via an intermediate mode (cavity mode) based on the optomechanical interaction.

Here we should point out that, to gain a high enough level of approximation, the perturbation series in Eq. (A4) has been truncated up to $j \leqslant 10$ during calculation of the analytical solution.

APPENDIX B: CHOICE OF THE SIDEBAND-MODULATION STRENGTHS FOR EXTERNAL DRIVING $\varepsilon_L(t)$ TO FULFILL THE DESIRED $G(t)$

To fulfill the desired form of the effective optomechanical coupling $G(t)$ in Eq. (7) when the set (G_{-1}, G_0, G_1) is given, the corresponding sideband-modulation strengths $(\varepsilon_{-1}, \varepsilon_0, \varepsilon_1)$ for the external driving $\varepsilon_L(t)$ can be derived analytically via Laplace transform,

$$\begin{aligned}
\varepsilon_{-1} &= \frac{G_{-1}}{g_0}\left[i(\Omega+\delta_a)+\frac{\kappa}{2}\right] \\
&\quad - i[2k_0G_{-1}+(k_3+k_4)G_0+(k_1+k_2)G_1], \\
\varepsilon_0 &= \frac{G_0}{g_0}\left(i\delta_a+\frac{\kappa}{2}\right) \\
&\quad - i[(k_3+k_4)G_{-1}+2k_0G_0+(k_3+k_4)G_1], \\
\varepsilon_1 &= \frac{G_1}{g_0}\left[i(\delta_a-\Omega)+\frac{\kappa}{2}\right] \\
&\quad - i[(k_1+k_2)G_{-1}+(k_3+k_4)G_0+2k_0G_1], \qquad \text{(B1)}
\end{aligned}$$

where

$$\begin{aligned}
k_0 &= -\frac{i\left(G_{-1}^2+G_0^2+G_1^2\right)}{2g_0S_1}, \\
k_1 &= -\frac{iG_{-1}G_1S_2}{g_0(S_1-S_2)(S_2-S_3)}, \\
k_2 &= \frac{iG_{-1}G_1S_3}{g_0(S_1-S_3)(S_2-S_3)}, \\
k_3 &= -\frac{iG_0(G_{-1}+G_1)S_4}{g_0(S_1-S_4)(S_4-S_5)}, \\
k_4 &= \frac{iG_0(G_{-1}+G_1)S_5}{g_0(S_1-S_5)(S_4-S_5)},
\end{aligned}$$

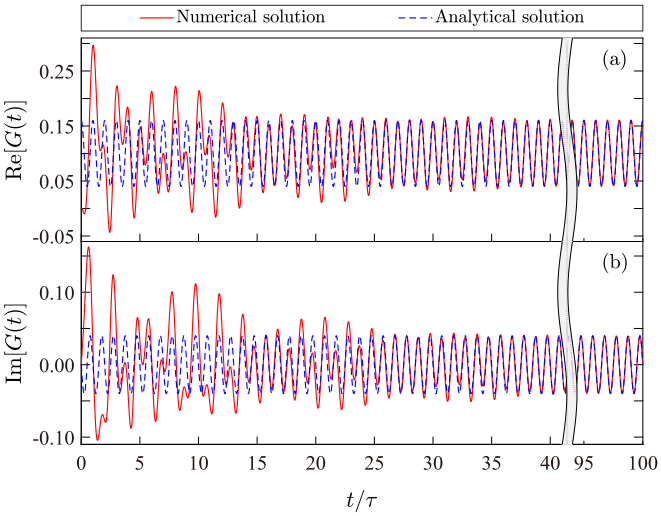

FIG. 11. Asymptotic time evolution of the real and imaginary parts (in units of ω_m) for the effective optomechanical coupling $G(t)$ in (a) and (b), respectively. The solid red curve shows the numerical result when the external periodic driving $\varepsilon_L(t) = \varepsilon_{-1}e^{i\Omega t} + \varepsilon_0 + \varepsilon_1 e^{-i\Omega t}$ is acting on the present optomechanical system, with the corresponding set of sideband-modulation strengths $(\varepsilon_{-1}, \varepsilon_0, \varepsilon_1)$ given in Eq. (B1). The dashed blue curve represents the analytical result obtained by the assumed $G(t)$ in Eq. (7). System parameters are as follows (in units of ω_m): $\gamma_m = 10^{-6}$, $\delta_a = 1$, $\kappa = 0.1$, $g_0 = 4\times10^{-6}$, $G_{-1} = 0.01$, $G_0 = 0.1$, and $G_1 = 0.05$.

$$\begin{aligned}
S_1 &= -i\omega_m - \frac{\gamma_m}{2}, \\
S_2 &= 2i\Omega, \quad S_3 = -2i\Omega, \\
S_4 &= i\Omega, \quad S_5 = -i\Omega. \qquad \text{(B2)}
\end{aligned}$$

To check the validity of the above-derived external periodic driving $\varepsilon_L(t)$, in Fig. 11 we compare the effective optomechanical coupling $G(t)$ obtained by, respectively, the numerical solution when $\varepsilon_L(t) = \varepsilon_{-1}e^{i\Omega t} + \varepsilon_0 + \varepsilon_1 e^{-i\Omega t}$ is applied to the present optomechanical system and the analytical solution assumed in Eq. (7). In Fig. 11, one can note that these two different kinds of solutions agree very well in modulation periods of $[95\tau, 100\tau]$. This means that the assumed effective optomechanical coupling form in Eq. (7) which is desired and necessary for the generation of mechanical squeezing can be precisely engineered in the long-time modulation limit via the choice of the suitable external driving-sideband strengths given in Eq. (B1).

[1] A. D. O'Connell, M. Hofheinz, M. Ansmann, R. C. Bialczak, M. Lenander, E. Lucero, M. Neeley, D. Sank, H. Wang, M. Weides, J. Wenner, J. M. Martinis, and A. N. Cleland, Nature **464**, 697 (2010).

[2] J. Chan, T. P. M. Alegre, A. H. Safavi-Naeini, J. T. Hill, A. Krause, S. Gröblacher, M. Aspelmeyer, and O. Painter, Nature **478**, 89 (2011).

[3] J. D. Teufel, T. Donner, D. Li, J. W. Harlow, M. S. Allman, K. Cicak, A. J. Sirois, J. D. Whittaker, K. W. Lehnert, and R. W. Simmonds, Nature **475**, 359 (2011).

[4] R. W. Peterson, T. P. Purdy, N. S. Kampel, R. W. Andrews, P. L. Yu, K. W. Lehnert, and C. A. Regal, Phys. Rev. Lett. **116**, 063601 (2016).

[5] J. B. Clark, F. Lecocq, R. W. Simmonds, J. Aumentado, and J. D. Teufel, Nature **541**, 191 (2017).

[6] H. Xu, L. Jiang, A. A. Clerk, and J. G. E. Harris, Nature **568**, 65 (2019).

[7] S. Gröblacher, K. Hammerer, M. R. Vanner, and M. Aspelmeyer, Nature **460**, 724 (2009).

[8] J. D. Teufel, D. Li, M. S. Allman, K. Cicak, A. J. Sirois, J. D. Whittaker, and R. W. Simmonds, Nature **471**, 204 (2011).

[9] D. Bothner, I. C. Rodrigues, and G. A. Steele, arXiv:1911.01262.

[10] M. Aspelmeyer, T. J. Kippenberg, and F. Marquardt, Rev. Mod. Phys. **86**, 1391 (2014).

[11] T. J. Kippenberg and K. J. Vahala, Science **321**, 1172 (2008).

[12] M. Aspelmeyer, P. Meystre, and K. Schwab, Phys. Today **65**, 29 (2012).

[13] M. Pierre, Ann. Phys. (Berlin) **525**, 215 (2013).

[14] W. H. Zurek, Phys. Today **44**, 36 (1991).

[15] K. C. Schwab and M. L. Roukes, Phys. Today **58**(7), 36 (2005).

[16] C. M. Caves, K. S. Thorne, R. W. P. Drever, V. D. Sandberg, and M. Zimmermann, Rev. Mod. Phys. **52**, 341 (1980).

[17] A. Abramovici, W. E. Althouse, R. W. P. Drever, Y. Gürsel, S. Kawamura, F. J. Raab, D. Shoemaker, L. Sievers, R. E. Spero, K. S. Thorne, R. E. Vogt, R. Weiss, S. E. Whitcomb, and M. E. Zucker, Science **256**, 325 (1992).

[18] G. Milburn and D. Walls, Opt. Commun. **39**, 401 (1981).

[19] D. Rugar and P. Grütter, Phys. Rev. Lett. **67**, 699 (1991).

[20] A. Mari and J. Eisert, Phys. Rev. Lett. **103**, 213603 (2009).

[21] J. Q. Liao and C. K. Law, Phys. Rev. A **83**, 033820 (2011).

[22] C. H. Bai, D. Y. Wang, S. Zhang, S. Liu, and H. F. Wang, Ann. Phys. (Berlin) **531**, 1800271 (2019).

[23] G. S. Agarwal and S. Huang, Phys. Rev. A **93**, 043844 (2016).

[24] B. Xiong, X. Li, S. L. Chao, and L. Zhou, Opt. Lett. **43**, 6053 (2018).

[25] K. Jähne, C. Genes, K. Hammerer, M. Wallquist, E. S. Polzik, and P. Zoller, Phys. Rev. A **79**, 063819 (2009).

[26] M. Asjad, G. S. Agarwal, M. S. Kim, P. Tombesi, G. Di Giuseppe, and D. Vitali, Phys. Rev. A **89**, 023849 (2014).

[27] S. Huang and G. S. Agarwal, Phys. Rev. A **82**, 033811 (2010).

[28] W. J. Gu, G. X. Li, and Y. P. Yang, Phys. Rev. A **88**, 013835 (2013).

[29] X. Y. Lü, J. Q. Liao, L. Tian, and F. Nori, Phys. Rev. A **91**, 013834 (2015).

[30] K. W. Xiao, N. Zhao, and Z. Q. Yin, Phys. Rev. A **96**, 013837 (2017).

[31] X. Han, D. Y. Wang, C. H. Bai, W. X. Cui, S. Zhang, and H. F. Wang, Phys. Rev. A **100**, 033812 (2019).

[32] C. H. Bai, D. Y. Wang, S. Zhang, S. Liu, and H. F. Wang, Photon. Res. **7**, 1229 (2019).

[33] A. A. Clerk, F. Marquardt, and K. Jacobs, New J. Phys. **10**, 095010 (2008).

[34] A. Szorkovszky, A. C. Doherty, G. I. Harris, and W. P. Bowen, Phys. Rev. Lett. **107**, 213603 (2011).

[35] A. Szorkovszky, G. A. Brawley, A. C. Doherty, and W. P. Bowen, Phys. Rev. Lett. **110**, 184301 (2013).

[36] R. Ruskov, K. Schwab, and A. N. Korotkov, Phys. Rev. B **71**, 235407 (2005).

[37] Z. C. Zhang, Y. P. Wang, Y. F. Yu, and Z. M. Zhang, Opt. Express **26**, 11915 (2018).

[38] A. Dalafi, M. H. Naderi, and A. Motazedifard, Phys. Rev. A **97**, 043619 (2018).

[39] X. You, Z. Li, and Y. Li, Phys. Rev. A **96**, 063811 (2017).

[40] L. T. Shen, X. Y. Chen, Z. B. Yang, H. Z. Wu, and S. B. Zheng, Phys. Rev. A **84**, 064302 (2011).

[41] K. W. Murch, U. Vool, D. Zhou, S. J. Weber, S. M. Girvin, and I. Siddiqi, Phys. Rev. Lett. **109**, 183602 (2012).

[42] N. Didier, F. Qassemi, and A. Blais, Phys. Rev. A **89**, 013820 (2014).

[43] S. L. Su, X. Q. Shao, H. F. Wang, and S. Zhang, Phys. Rev. A **90**, 054302 (2014).

[44] X. Q. Shao, Phys. Rev. A **98**, 042310 (2018).

[45] H. Tan, G. Li, and P. Meystre, Phys. Rev. A **87**, 033829 (2013).

[46] Y. D. Wang and A. A. Clerk, Phys. Rev. Lett. **110**, 253601 (2013).

[47] S. Barzanjeh, E. S. Redchenko, M. Peruzzo, M. Wulf, D. P. Lewis, G. Arnold, and J. M. Fink, Nature **570**, 480 (2019).

[48] M. J. Woolley and A. A. Clerk, Phys. Rev. A **89**, 063805 (2014).

[49] C. F. Ockeloen Korppi, E. Damskägg, J. M. Pirkkalainen, M. Asjad, A. A. Clerk, F. Massel, M. J. Woolley, and M. A. Sillanpää, Nature **556**, 478 (2018).

[50] A. Kronwald, F. Marquardt, and A. A. Clerk, Phys. Rev. A **88**, 063833 (2013).

[51] E. E. Wollman, C. U. Lei, A. J. Weinstein, J. Suh, A. Kronwald, F. Marquardt, A. A. Clerk, and K. C. Schwab, Science **349**, 952 (2015).

[52] J. M. Pirkkalainen, E. Damskägg, M. Brandt, F. Massel, and M. A. Sillanpää, Phys. Rev. Lett. **115**, 243601 (2015).

[53] C. U. Lei, A. J. Weinstein, J. Suh, E. E. Wollman, A. Kronwald, F. Marquardt, A. A. Clerk, and K. C. Schwab, Phys. Rev. Lett. **117**, 100801 (2016).

[54] A. Kronwald, F. Marquardt, and A. A. Clerk, New J. Phys. **16**, 063058 (2014).

[55] R. Zhang, Y. Fang, Y. Y. Wang, S. Chesi, and Y. D. Wang, Phys. Rev. A **99**, 043805 (2019).

[56] X. W. Xu and Y. Li, Phys. Rev. A **91**, 053854 (2015).

[57] D. Vitali, S. Gigan, A. Ferreira, H. R. Böhm, P. Tombesi, A. Guerreiro, V. Vedral, A. Zeilinger, and M. Aspelmeyer, Phys. Rev. Lett. **98**, 030405 (2007).

[58] P. Rabl, Phys. Rev. Lett. **107**, 063601 (2011).

[59] C. W. Gardiner and P. Zoller, *Quantum Noise*, 3rd ed. (Springer, New York, 2004).

[60] G. Teschl, *Ordinary Differential Equations and Dynamical Systems* (American Mathematical Society, 2012).

[61] E. X. DeJesus and C. Kaufman, Phys. Rev. A **35**, 5288 (1987).

[62] M. O. Scully and M. S. Zubairy, *Quantum Optics* (Cambridge University Press, Cambridge, UK, 1997).

[63] S. Chakraborty and A. K. Sarma, Phys. Rev. A **97**, 022336 (2018).

[64] W. Vogel and D. G. Welsch, *Quantum Optics* (Wiley-VCH, Weinheim, 2006).

[65] C. Weedbrook, S. Pirandola, R. García-Patrón, N. J. Cerf, T. C. Ralph, J. H. Shapiro, and S. Lloyd, Rev. Mod. Phys. **84**, 621 (2012).

[66] A. Mari and J. Eisert, New J. Phys. **14**, 075014 (2012).

[67] Y. C. Liu, R. S. Liu, C. H. Dong, Y. Li, Q. Gong, and Y. F. Xiao, Phys. Rev. A **91**, 013824 (2015).

[68] D. G. Lai, F. Zou, B. P. Hou, Y. F. Xiao, and J. Q. Liao, Phys. Rev. A **98**, 023860 (2018).

[69] D. Y. Wang, C. H. Bai, S. Liu, S. Zhang, and H. F. Wang, Phys. Rev. A **98**, 023816 (2018).

[70] A. Farace and V. Giovannetti, Phys. Rev. A **86**, 013820 (2012).

[71] M. Schmidt, M. Ludwig, and F. Marquardt, New J. Phys. **14**, 125005 (2012).